High Resolution DEM Building with SAR Interferometry and High Resolution optical Image

Omar HADJ-SAHRAOUI [a]
[a] *Remote Sensing department, Algerian Space Agency, 01 Avenue de la Palestine, B.P.13 Arzew, Oran, Algérie*
sahraoui_omar1@yahoo.fr
Tel. : 00 213 90 61 27 90 – Fax :00 213 41 47 36 65
Hadria FIZAZI [b]
[b] *Computer Science department, University of Sciences and Technology Oran*
hadria.fizazi@yahoo.fr
Faouzi BERRICHI [a],
[a] Remote Sensing department, Algerian Space Agency, 01 Avenue de la Palestine, B.P.13 Arzew, Oran, Algérie
f.algeria@gmail.com
Tel. : 00 213 90 61 27 90 – Fax :00 213 41 47 36 65
Djemoui CHAMAKHI [a]
[a] *Remote Sensing department, Algerian Space Agency, 01 Avenue de la Palestine, B.P.13 Arzew, Oran, Algérie*
djimoui@yahoo.com
Tel. : 00 213 90 61 27 90 – Fax :00 213 41 47 36 65
Lahcen KEBIR [a]
[a] *Remote Sensing department, Algerian Space Agency, 01 Avenue de la Palestine, B.P.13 Arzew, Oran, Algérie*
wahib_kdz@yahoo.fr
Tel. : 00 213 71 59 74 16 – Fax :00 213 41 47 36 65

Abstract: There have been many published articles describing Interferometry algorithms for DEM generation in different applications. The best uncertainty achieved in most of these articles is greater than ±1m calculating the elevation. Enabling scientists to gain experience with new techniques at low cost. Synthetic aperture radar interferometry (InSAR) is an imaging technique for measuring the topography of a surface, its changes over time, and other changes in the detailed characteristics of the surface [9].

To take a better resolution of the surfaces, we propose our approach; it's to merge the results of the interferometry and data from segmentation of an optical high resolution image.

In this report we describe a procedure for hybridization of interferometry Algorithm (InSAR) and the use of geospatial data from the image segmentation, with Extraction of the building to calculate the zonal statistic parameter and mapping all segments comprising the highest elevations.

This report is written in a step by step format to simplify the complicated steps described in the paper, with a focus on the Hybridization instead of the interferometry. The tests of this method were carried out on several sites, and showed good results.

Keywords : InSAR Interferometry, co-registration, Building High resolution, hybridization, interferometric coherence, DEM Building.

Introduction:

With the continuous technological advancements in Interferometry applications, there will always be a demand for smaller uncertainty in calculating the high resolution pixels. Many methods to calculate the High resolution InSAR have been published in the Interferometry literature, nevertheless, their uncertainties have been in planimetry and altimetry calculations, and some are only valid for a specific images or images with the best coherence.

Description of the process:

This article describes the process that allows the realization of a DEM by the INSAR technique and merges it with information extracted from the data of very high resolution. The process description shows a variety of instructions by a series of steps; on otherwise, the description of the mechanism focuses on the object of the buildings.

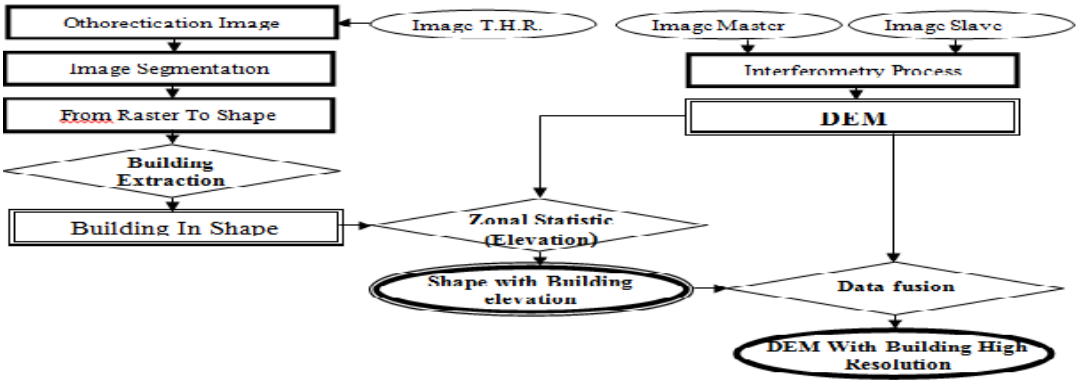


Figure 1: Graph of the global approach for DEM computing

SAR Interferometry for DEM Generation [9]:

Two SAR images are combined to produce a SAR Interferogram to reveal information about the third dimension (elevation) of the object and to measure small displacements of objects between the two image acquisitions. An interferogram is an image acquired by making the phases of two SAR images of the same ground to interfere [9].

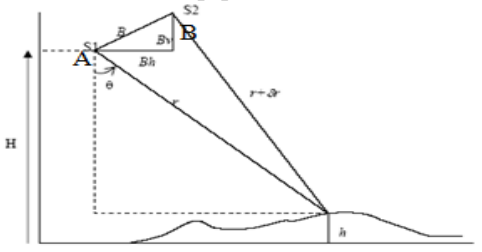


Figure 2 : InSAR Geometry

Thus, after registration, the complex interferograms are formed by multiplying each complex pixel of the first image by the complex conjugate of the same pixel in the second image. The result interferogram thus generated is a complex image, its intensity is a measure of cross correlation of the images (Magnitude), and its phase is a result of several parameters including the topographical changes or height variations Represented by fringes [9].

The phase difference ϕ between two acquisitions signals related the same object. It's calculated by the following expression:

$$\psi(i,j) = A(i,j)B^*(i,j)| = \rho_A(i,j)\rho_B(i,j)e^{j(\phi_A(i,j)-\phi_B(i,j))} \quad (1.\ a)$$

Where (A S_1, B S_2) are the two master and slave images and (ρ_A,ρ_B)(ϕ_A,ϕ_B) are respectively the modules and the arguments of the images A and B. and developed by the expression With:

$$\phi = \frac{4\pi(\delta r)}{\lambda} = \frac{4\pi(B_h \sin\theta - B_v \cos\theta)}{\lambda} \quad (1)$$

- λ : the wavelength,
- δr : Range difference,
- Bh: Horizontal baseline,
- Bv : Vertical baseline,
- θ : look angle.

Based on the look angle and range difference changes, the interferogram can be generated as:

$$\Delta h = \frac{\lambda r \sin\theta}{4\pi B}\Delta\phi \quad (2)$$

- r : Range of image A,
- $\Delta\phi$: Phase between A and B,
- B : Base line(normal)

The description of Interferometry chains is given by this algorithm [9]:

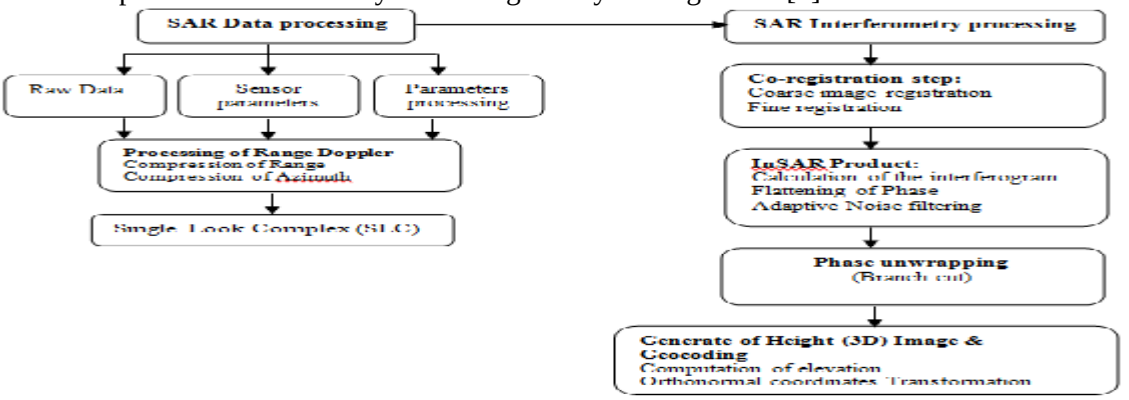


Figure 3: InSAR processing organization

InSAR processing:

***Step 1*: Image Co-registration**

The first step and the most essential in the InSAR process is the Co-registration. InSAR complex data processing combines SLCI images for SAR interferogram generation. The Precise co-registration with great correlation of InSAR coherence is crucial and indispensable for this step.

By modeling the two SAR images with random complex signals zM and zS centered and jointly stationary in the broad sense (laws independent of the position in the image), In such ways the phase difference and consistency are defined from the normalized correlation [6] [7] [8]:

$$C = \rho e^{j\phi} = \frac{E\{z_M z_S^*\}}{\sqrt{E\{|z_M|^2\}E\{|z_S|^2\}}} \quad (3)$$

We interested to the fine co-registration after a global coregistration, to estimate the offset error. With different equations [1] [2] [3]:

$$\varepsilon_{\text{recalage}} = \frac{\delta(R_2 - R_1)}{\delta d} - \frac{\overline{\delta(R_2 - R_1)}}{\delta d} \approx \frac{1}{k_\alpha}\frac{b}{R}\left(\frac{\cos(\theta - \alpha_b)}{\tan(\theta - \alpha_a)} - \frac{\cos(\theta - \alpha_b)}{\tan(\theta)}\right) \quad (4)$$

$$\varepsilon_{\text{recalage}} \approx \frac{1}{k_\alpha}\frac{b}{R}\cos(\theta - \alpha_b)\left(\frac{\cos(\theta - \alpha_a)}{\sin(\theta - \alpha_a)} - \frac{\cos(\theta)}{\sin(\theta)}\right) \quad (5)$$

$$\varepsilon_{\text{recalage}} \approx \frac{1}{k_\alpha}\frac{b}{R}\cos(\theta - \alpha_b)\frac{\sin(\theta)\cos(\theta - \alpha_a) - \cos(\theta)\sin(\theta - \alpha_a)}{\sin(\theta)\sin(\theta - \alpha_a)} \quad (6)$$

$$\varepsilon_{recalage} \approx \frac{1}{k_{\alpha}} \frac{b}{R} \cos(\theta - \alpha_b) \frac{\sin(\alpha_a)}{\sin(\theta)\sin(\theta \quad \alpha_a)} \qquad (7)$$

Step 2: **Interferogram generation**

In order to be able to calculate the 3rd dimension, it is necessary to arrange the two phases of SAR images on the same terrain and focus in the same view, by the application of the coarse registration in the first step and refine it by interpolation (Fine-registration) in second step. After the co-registration process, the interferometer is produced by the multiplication of each selected pixel of the SLC first by the second conjugate of the same pixel. The interferogram intensity is estimated by cross correlation of the SLCI images.

the coherence ρ is related to the normalized correlation of the intensities and It is given by the following formulation [4] [5]*:*

$$\rho = \begin{cases} \sqrt{2\gamma_I - 1} & \gamma_I \geq 1/2 \\ 0 & \gamma_I < 1/2 \end{cases} \qquad (8)$$

With:

$$\gamma_I = \frac{\sum_{i=1}^{L} |u_1(i)|^2 |u_2(i)|^2}{\sqrt{\sum_{i=1}^{L} |u_1(i)|^4 \sum_{i=1}^{L} |u_2(i)|^4}} \qquad (9)$$

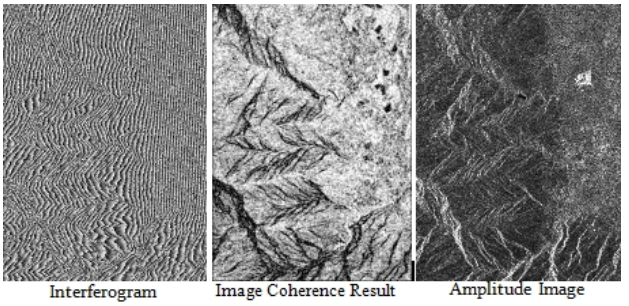


Figure 4: result of co-registration for Interferogram & coherence images

To continue with the unwrapping process, it's necessary to remove the orbital fringes and the fringes of the flat earth. And in second step to reduce the noise on the phase interferogram by an adaptive filter application. (The same zoom of different figures).

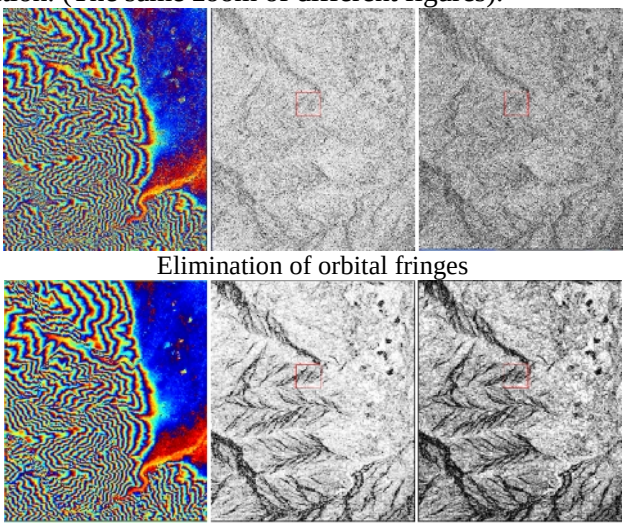


Figure 5: Elimination of orbital fringes applying the filter on the interferogram

Step 3: **Phase unwrapping**

The interferogram produced by the interferometry is given unfortunately by a phase value for each pixel at the modulo 2π which means that the supplied phase value is between $\phi \in [0,2\pi]$, while the true value may exceed 2π.

The measurement of the corresponding elevation is therefore ambiguous. This problem must be solved by a phase unwrapping step, which for the interferometry technique is a necessary for DEM generation. This step is considered the most delicate in rough terrain, building and steep slopes or discontinuities surfaces.

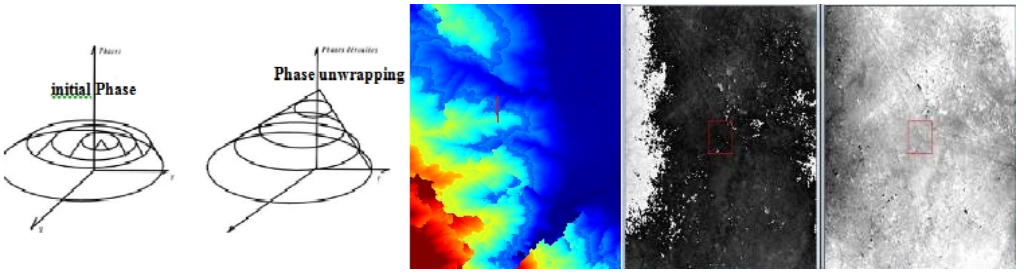


Figure 6: unwrapping phase & Interferogram filtered.

Step 4: **Height map generation & Geocoding**

In this step, we convert the value of unwrapped phase to elevation for each calculated pixel value form the necessary DEM images generate. The L-look interferometric phase Φ and the corresponding coherence ρ are defined by [1] [4] [5] [6] [7] [8]:

$$\rho e^{j\Phi} = \frac{\left(\sum_{n=1}^{L} s_1(n)\right)\left(\sum_{n=1}^{L} s_2^*(n)\right)}{\sqrt{\sum_{n=1}^{L}|s_1(n)|^2 \sum_{n=1}^{L}|s_2(n)|^2}} \quad (10)$$

Relative height *h* and interferometric phase are linked by the following relation:

$$h = \frac{\lambda}{2\pi}\frac{R\sin(\theta)}{B_{\perp}}\Phi \quad (11)$$

With R is the mean distance between sensors and the target; $\beta_{\perp}$ is the orthogonal projection of the baseline (distance between the two sensors) on the perpendicular direction to the propagation axis; the λ is wavelength and the θ is viewing angle.

The coordinate system of the synthetic aperture radar generate orthocorrected DEM by InSAR Technique, with projection and cartographic orientation

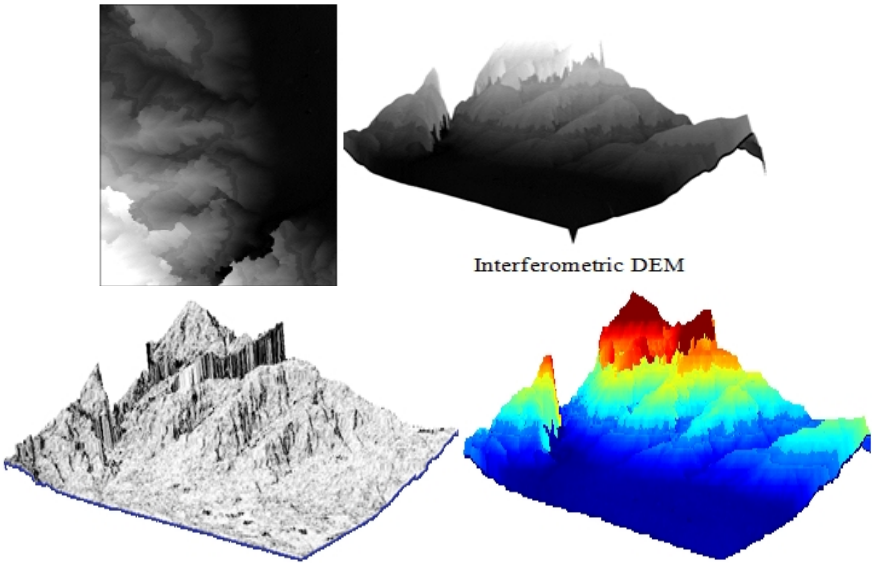


Figure 7: Interferometric DEM.

Orthorectification:

Before segmenting the image to proceed with the extraction of the building, it's necessary to keep the same geometric forms of objects (between Image and DEM) and to be able to merge the building image with the generated DEM, it is necessary to apply the orthorectification of the image of very high resolution.

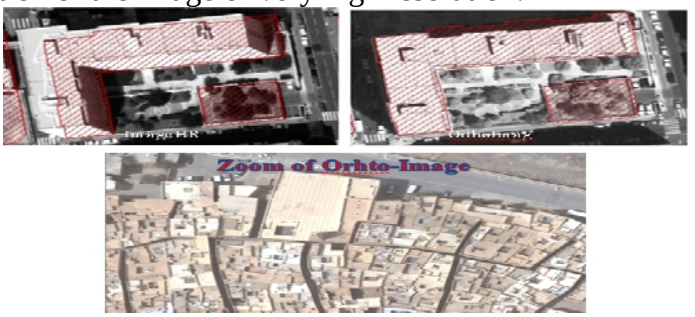


Figure 8: Process of Orthorectifation Image.

Mean shit Segmentation of the very high resolution image:

This process of Mean-Shift segmentation is performed on very high resolution panchromatic or multispectral images, of which two different modes can be used as output (vector or raster). Not only the robustness of this segmentation algorithm, then you can load, run the segmentation algorithm with all required parameters, vectorize and store in the output file or database.

The very high resolution images are voluminous, so the Mean-Shift algorithm deflects the image into several small mosaic images called Tuille, in order to be able to process them sequentially and quickly.

Among the strong points of this process is the Stitch option, which makes it possible to unite the segments of the same nature and even for the segments of the adjacent tiles. This option allows defining the minimum size of the smallest segments, to combine these small segments with their significant segments.

The Mean-Shift Process:

•Initialize: Set X to the value of the point to classify
•Repeat:
- Move X by the corresponding mean shift vector:

$$X \leftarrow X + M(X) = \frac{\sum_i X_i g\left(\frac{\|X - X_i\|^2}{h^2}\right)}{\sum_i g\left(\frac{\|X - X_i\|^2}{h^2}\right)} \qquad (12)$$

•Until X converges
•Note: Convergence is guaranteed.

Mean Shift Segmentation Algorithm :

- For each $i= 1…n$ run the mean shift procedure for x_i and store the convergence point in z_i.
- Identify clusters $\{Cp\}_{p=1…m}$ of convergence points by linking together all z_i which are closer than 0,5 from each other in the joint domain.
- For each $i= 1…n$ assign $L_i= \{p \mid z_i \epsilon C_p\}$.
- Optional: Eliminate spatial regions smaller than
- M pixels.

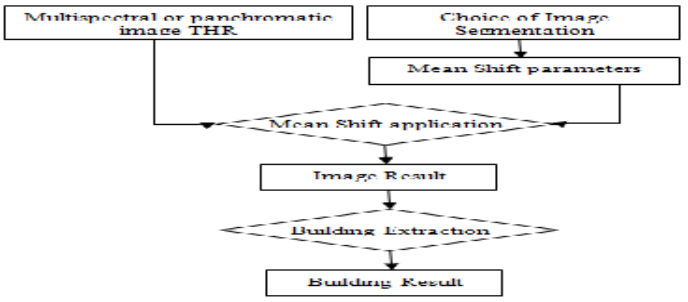


Figure 9: Mean Shift process organization

For the same process in raster mode, the result obtained is a segmented image with a label which allows the identification of the regions. In this raster mode, there is the Color Mapping tool with look-up table calculated on support image to render regions with contrasted colors. And we take the output with same Color of the support image.

We present an extract of zoom on the source image and of the segmented image, in the following figure:

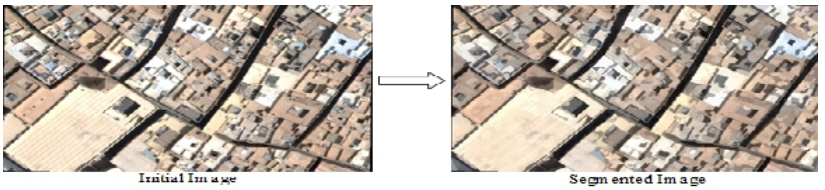


Figure 10: Mean Shift Segmentation result.

Polygonize the segmented image and extraction of the building:

Converting between raster file and vector formats allows you to make use of both raster and vector data when solving a GIS problem or modify the new vector file, as well as using the various tools and analysis methods unique to these two forms of geographic data. This increases the flexibility you have when considering data sources and processing methods for solving a GIS problem.

The goal for this process is, to get the raster result into a vector that can be used to complete the analysis of building Extraction.

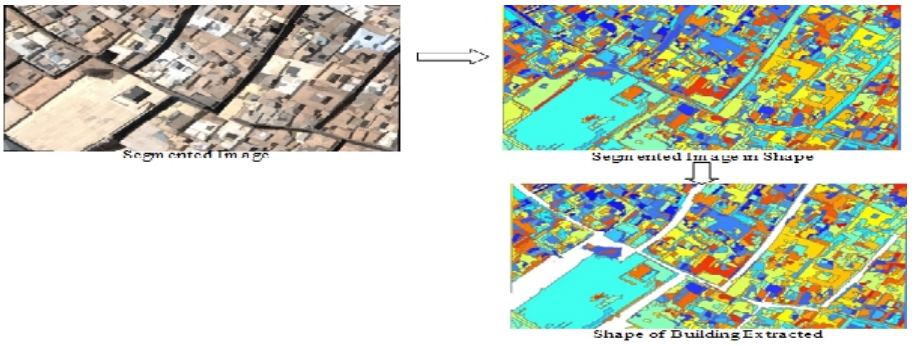
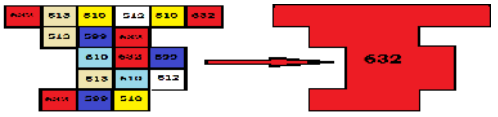


Figure 11: From Raster Image to Shape vector form for Building Extraction vector.

Zonal Statistics Process:



To compute the statistics of the maximum elevation of each building polygon from InSAR DEM value, we used the Zonal Statistics tool. This tool produces a single value of the DEM

surface dataset for each polygon produced by Mean Shift Segmentation of High Resolution optical Image.

This figure illustrate the extraction of the maximum elevation parameter of DEM areas by Building polygons, in order to generate a new database specific to the new DEM elevations that come back to update the InSAR DEM.

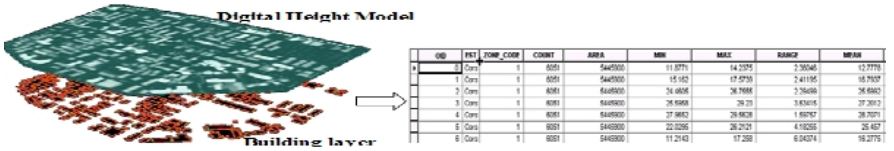


Figure 12: Zonal statistic Result and Data Base realization.

DEM Building Result:

With a crossing of the results obtained by the InSAR and the statistics of the zones, it obtains a final result on the DEM with very high resolution beam.

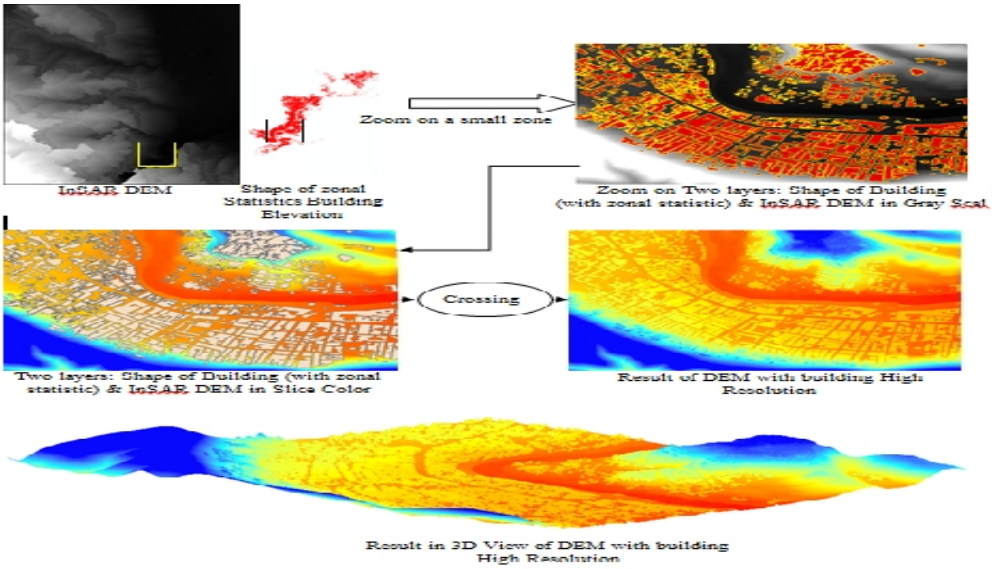


Figure 13: Final result in 2D and 3D view.

Conclusion:

The addition of geospatial capabilities to InSAR Interferometry through the Image High resolution allows the user to process and visualize the spatial distribution of DEM with high resolution building results. Because of the availability of digital terrain data and processing capabilities, GIS is well suited to assist in performing crossing layers analysis.

The union of the very high resolution imagery and the radar interferometry gives an acceptable result in the building zones.

REFERENCES :

[1]. **CELINE TISON, FLORENCE TUPIN, AND HENRI MAITRE,** A Fusion Scheme for Joint Retrieval of Urban Height Map and Classification From High-Resolution Interferometric SAR Images, IEEE TRANSACTIONS ON GEOSCIENCE AND REMOTE SENSING, VOL. 45, NO. 2, FEBRUARY 2007

[2]. **ARGUS, D., M. HEFLIN, G. PELTZER, F. CRAMPE, AND F. WEBB**, Interseismic strain accumulation and anthropogenic motion in metropolitan Los Angeles, J. Geophys. Res., 110, B04401, doi:10.1029/2003JB002934, 2005.

[3]. **BAKER, S. AND AMELUNG**, F., 2012, Top-down inflation and deflation at the summit of Kilauea Volcano, Hawaii observed with InSAR, Journal of Geophysical Research: Solid Earth, v.117, DOI: 10.1029/2011JB009123

[4]. **GRAHAM** C, juin 1974. *Synthetic interferometer Radar fot Topographic Mapping*, Proceedings of The IEEE, Vol 62, p763.

[5]. **KENYI L & RAGGAM H**, 1996. *Accuracy assessment of interferometrically derived DTMs*, FRINGE96

[6]. **MASSONNET D & FEIGL K**, 04/11/1998. *Radar Interferometry and its application to changes in the earth's surface, Reviews of Geophysics*, vol 36, p441-500.

[7]. **U. Stilla, U. Soergel, and U. Thoennessen**, "Potential and limits of InSAR data for building reconstruction in built-up areas," *ISPRS Journal of Photogrammetry and Remote Sensing*, pp. 113–123, May 2003.

[8]. **C. Chesnaud, P. Réfrégier, and V. Boulet**, "Statistical region snake- based segmentation adapted to different physical noise models," *IEEE Transactions on Pattern Analysis and Machine Intelligence*, vol. 21, no. 11, pp. 1145–1157, Nov. 1999.

[9]. O. Hadj Sahraoui, B. Hassaine, C. Serief, "Radar Interferometry with Sarscape Software", www.creaso.com, SARScape 2006/2007.